AGU PUBLICATIONS

Geophysical Research Letters

RESEARCH LETTER
10.1002/2016GL068827

Key Points:
- Significant correlation between reconstructed subduction of the last 130 Myr and mantle structure at 600 to 2300 km depth
- Further correlation (beyond 2300 km/130 Ma) not presently demonstrable due to uncertainties in tomographic and paleogeographic models
- Subducted slabs sink through the lower mantle, on average, at rates between 1.1 and 1.9 cm yr^{-1}

Supporting Information:
- Supporting Information S1

Correspondence to:
M. Domeier,
mathew.domeier@geo.uio.no

Citation:
Domeier, M., P. V. Doubrovine, T. H. Torsvik, W. Spakman, and A. L. Bull (2016), Global correlation of lower mantle structure and past subduction, *Geophys. Res. Lett.*, *43*, 4945–4953, doi:10.1002/2016GL068827.

Received 4 APR 2016
Accepted 4 MAY 2016
Accepted article online 7 MAY 2016
Published online 23 MAY 2016

Global correlation of lower mantle structure and past subduction

Mathew Domeier[1], Pavel V. Doubrovine[1], Trond H. Torsvik[1,2,3], Wim Spakman[1,4], and Abigail L. Bull[1]

[1]Centre for Earth Evolution and Dynamics, University of Oslo, Oslo, Norway, [2]Geodynamics, Geological Survey of Norway, Trondheim, Norway, [3]School of Geosciences, University of Witswatersrand, Johannesburg, South Africa, [4]Department of Earth Sciences, University of Utrecht, Utrecht, Netherlands

Abstract Advances in global seismic tomography have increasingly motivated identification of subducted lithosphere in Earth's deep mantle, creating novel opportunities to link plate tectonics and mantle evolution. Chief among those is the quest for a robust subduction reference frame, wherein the mantle assemblage of subducted lithosphere is used to reconstruct past surface tectonics in an absolute framework anchored in the deep Earth. However, the associations heretofore drawn between lower mantle structure and past subduction have been qualitative and conflicting, so the very assumption of a correlation has yet to be quantitatively corroborated. Here we show that a significant, time-depth progressive correlation can be drawn between reconstructed subduction zones of the last 130 Myr and positive *S* wave velocity anomalies at 600–2300 km depth, but that further correlation between greater times and depths is not presently demonstrable. This correlation suggests that lower mantle slab sinking rates average between 1.1 and 1.9 cm yr^{-1}.

1. Introduction

Conventionally, global paleogeographic reconstructions extending back into the mid-Early Cretaceous have been built through the combined use of marine magnetic anomalies, which reflect relative plate motion, and hotspot tracks, which describe the absolute motion of plates with respect to hotspots assumed to be sourced by plumes from the deep mantle [*Doubrovine et al.*, 2012; *Seton et al.*, 2012]. By unifying the relative plate circuits with the absolute motions established from hotspot tracks, the constituent motions of the entire plate system can be reexpressed with respect to the underlying mantle, thus allowing one to consider and model the geodynamic linkages between the surface and deep Earth. However, owing to the incessant loss of oceanic lithosphere to subduction, the data constraining hotspot reference frames become less abundant with age and can only be extended back to ~130 Ma, with notably large uncertainties already present before the mid-Late Cretaceous (83.5 Ma). For earlier times, paleogeographic reconstructions are assembled from paleomagnetic data, which record the latitudinal and azimuthal positions of crustal blocks, but do not constrain paleolongitude and, unlike hotspot tracks, need to be corrected for true polar wander [*Goldreich and Toomre*, 1969] to allow restoration to the mantle reference frame [*Torsvik et al.*, 2012]. Yet the determination and correction for true polar wander requires information about paleolongitude, so for times prior to the mid-Early Cretaceous the construction of a global plate model referenced to the mantle has long proven to be an intractable problem.

This longitudinal uncertainty could be overcome with a subduction reference frame, wherein the locations of former subduction zones (and thus their associated plates) are estimated from the occurrence of subducted lithosphere at varying depths in the mantle, as identified by seismic tomography [*van der Meer et al.*, 2010]. However, the underlying assumption of this approach—namely, that there exists a relation between global seismic mantle structure and the history of subduction—has never been validated. *Van der Meer et al.* [2010] presented a global catalog of seismic *P* wave velocity anomalies interpreted as oceanic lithosphere subducted in the last ~250 Myr and attributed them to past subduction-related orogenic events, leading to a subduction reference framework from which an average slab sinking rate of 1.2 ± 0.3 cm yr^{-1} was estimated; but their correlations were qualitative and presupposed. Earlier quantitative analyses of mantle structure and past subduction used either depth-integrated mantle structure [*Richards and Engebretson*, 1992] or a time-integrated subduction history [*Scrivner and Anderson*, 1992], thereby limiting inferences on time-depth trends. *Wen and Anderson* [1997] conducted the first and only quantitative comparison between mantle structure and paleo-subduction using discrete reconstruction times and discrete mantle depths. They reported an excellent correlation between paleo-subduction (30–130 Ma) and positive seismic velocity anomalies at 800–1100 km depth but could not otherwise recognize a progressive time-depth relationship between them.

Here we develop a statistical approach and reconsider the correlation between lower mantle structure and past subduction by comparing the time-dependent subduction history (back to 200 Ma) from the original model of *Seton et al*. [2012] with the depth-dependent seismic velocity structure of 10 *S* wave mantle tomography models and two composite (mean) models. Importantly, the outcome of our analysis is implicitly dependent on the assumption that the tomography and plate models are approximate realizations of true mantle structure and global tectonic evolution, respectively, and large deviations therein will expectedly reduce or obscure the observed correlation, without physical meaning. This is especially relevant for the plate model with its increasing uncertainty prior to the mid-Late Cretaceous.

2. Materials and Methods

Due to significant differences in the inferred mantle structure among contemporary global tomography models, we have considered a variety of global *S* wave velocity models (which provide a better global coverage than contemporary *P* wave velocity models), namely, gypsums [*Simmons et al*., 2010], hmsl-s [*Houser et al*., 2008], ngrand [*Grand*, 2002], pri-s05 [*Montelli et al*., 2006], s40rts [*Ritsema et al*., 2011], 362ani [*Kustowski et al*., 2008], savani [*Auer et al*., 2014], saw24b16 [*Mégnin and Romanowicz*, 2000], sb4l18 [*Masters et al*., 2000], and tx2007 [*Simmons et al*., 2007], in addition to two mean *S* wave tomography models, s5mean and s10mean [*Doubrovine et al*., 2016]. Following the methodology of *Becker and Boschi* [2002], *Doubrovine et al*. [2016] constructed s5mean by averaging gypsums, hmsl-s, s40rts, 362ani, and saw24b16, whereas s10mean was constructed from the averaging of all 10 of the aforementioned *S* wave models. These mean tomography models can be considered as robust smoothed averages of mantle structure. From each tomography model we extracted the seismic velocity fields in spherical layers at 100 km intervals between 600 and 2800 km depth. The mean seismic velocity of each layer was removed so that the velocity perturbations ($\delta \ln V_S$) used in our analyses were referenced to the local (layer-dependent) mean. Removal of the layer-dependent means does not change the relative velocity structure (in which we are interested herein) and at the same time allows us to directly compare the results from the various tomography models, which is otherwise not possible as they do not all adopt the same 1-D reference model.

For the plate tectonic model, the original model of *Seton et al*. [2012] was selected because it is the first and only documented global plate model constructed with continuously closing plate polygons [*Gurnis et al*., 2012] for the time interval 0–200 Ma. The continuously closing plate polygons are built from positionally dynamic boundaries that are defined continuously in time, such that the geometry and kinematics of the resulting plates can be queried at any arbitrary temporal scale, unlike conventional plate models which are constructed in static time steps (usually several tens of million years). The plate model is likewise continuously defined spatially, so that the plates and plate boundaries can be queried at any arbitrary spatial scale. Regional updates to this plate model [e.g., *Zahirovic et al*., 2014] were not used because their construction was informed by tomographic data, thus removing the mutual independence between tomography and the plate reconstructions that is required for us to meaningfully compare them. To determine the location of subduction through time in the plate model, we first seeded the boundaries of each time-dependent polygon with a high density of additional nodes and then calculated the magnitude of convergent, divergent, and transform motion at each node in 1 Myr intervals. The locations of subduction were then defined by the locations of convergent nodes. To reduce noise introduced from imperfections in the plate model, we exclude all convergent nodes where relative motion is greater than 80% transcurrent or where total convergence is less than 0.1° Myr^{-1}, as averaged over the 1 Myr sampling interval. Notably, some imperfections in the plate model are not eliminated by these thresholds (for example, the convergent cells in the southern Atlantic in Figure 1). The effects of more aggressive filtering are explored in section 5. To be comparable with the sampling frequency we used for the tomography models (which yielded 23 layers), we extracted the reconstructed subduction locations in 10 Myr intervals between 10 and 200 Ma.

Because we consider possible variations in correlation with a temporal resolution of 10 Myr, we wish to preserve subtle differences in reconstructed subduction locations between time steps and thus opt for a grid-based analysis. The time-dependent convergent nodes from the plate model (for each reconstruction age) and the layer-dependent $\delta \ln V_S$ data from the tomographic models (for each depth) were therefore resampled to the geographic grid at 1° intervals.

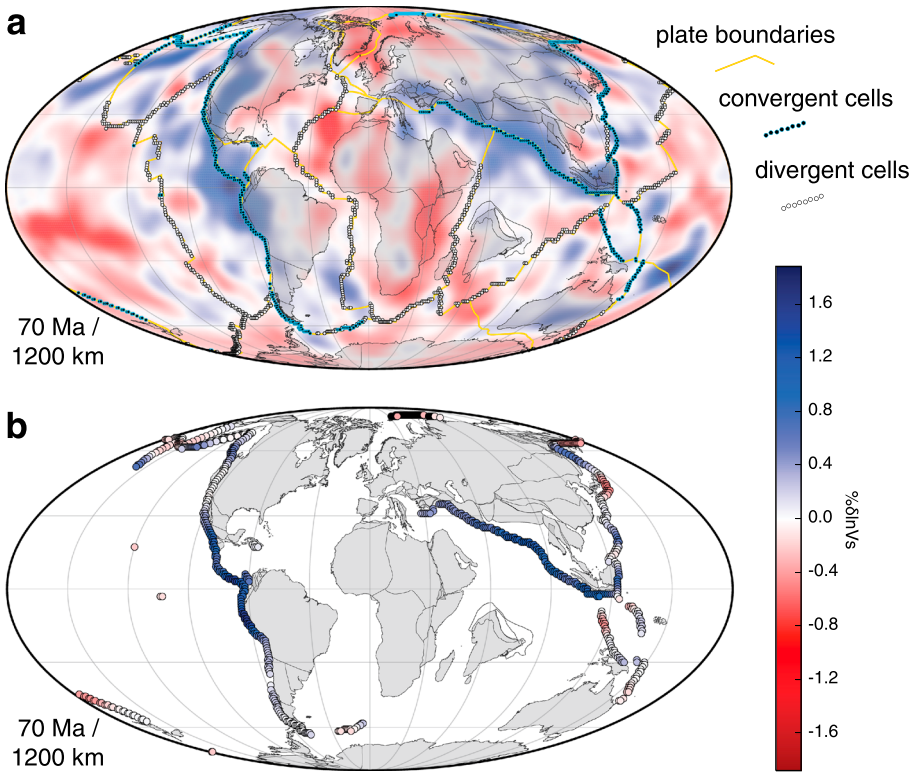

Figure 1. (a) An example comparison between reconstructed subduction locations (at 70 Ma; *Seton et al.* [2012]) and *S* wave tomography (at 1200 km; s10mean model [*Doubrovine et al.*, 2016]). (b) $\delta \ln V_S$ values from 1200 km depth projected onto the locations of convergence at 70 Ma, allowing calculation of an average $\delta \ln V_S$ value for this particular time-depth comparison (70 Ma versus 1200 km).

3. Initial Comparisons

As a first, simple experiment, we compare locations of subduction zones at each time *t* (10 to 200 Ma in 10 Myr increments) against surface-projected seismic velocity perturbations ($\delta \ln V_S$) in the lower mantle at each depth *d* (600 to 2800 km depth in 100 km increments) and calculate the average $\delta \ln V_S$ per subduction cell (from 1° cells on the geographic grid) for each *t-d* combination in each of the tomographic models (Figure 1). The average $\delta \ln V_S$ per subduction cell (hereafter "average $\delta \ln V_S$") is computed from all $\delta \ln V_S$ values in layer *d* that occupy a grid cell where subduction was occurring, according to the distribution of subduction grid cells in reconstruction *t*, and they are weighted by the area of their respective grid cells (or the cosine of latitude). If positive values of $\delta \ln V_S$ manifest the presence of colder, subducted lithosphere, as is commonly assumed, and slabs sink near vertically, we expect the reconstructed subduction geometries to best align with positive $\delta \ln V_S$ values for those *t-d* combinations which most closely correspond to the global average sinking velocity of slabs. To free the analysis from any a priori assumptions about slab sinking rates, all *t-d* combinations are considered. Figure 2 shows that this experiment yields a positive average $\delta \ln V_S$ for *all t-d* comparisons for the mean tomography models (s5mean and s10mean), even for those which would imply a geodynamically unreasonable slab sinking rate (up to 28 cm yr^{-1}). Also shown in Figure 2 are the depth-dependent normalizations of the *t-d* comparisons, wherein the average $\delta \ln V_S$ values (for all times *t*) at the same depth *d* are normalized by the maximum absolute average $\delta \ln V_S$ value at depth *d*. In this way the strongest average $\delta \ln V_S$ values are highlighted at each depth (the largest average $\delta \ln V_S$ value at each depth is also indicated by best fit *t-d* curves). The collected *t-d* comparisons for the individual tomography models and their depth-dependent normalizations are presented in the supporting information (Figure S1).

One explanation for the invariably positive average $\delta \ln V_S$ values observed in Figure 2 is that many of the major subduction zones of the last 200 Myr have migrated little with respect to the large positive seismic velocity anomalies as they are presently imaged (Figure 3). In other words, a slab sinking near vertically beneath a relatively stationary trench would expectedly yield a range of apparently positive time-depth

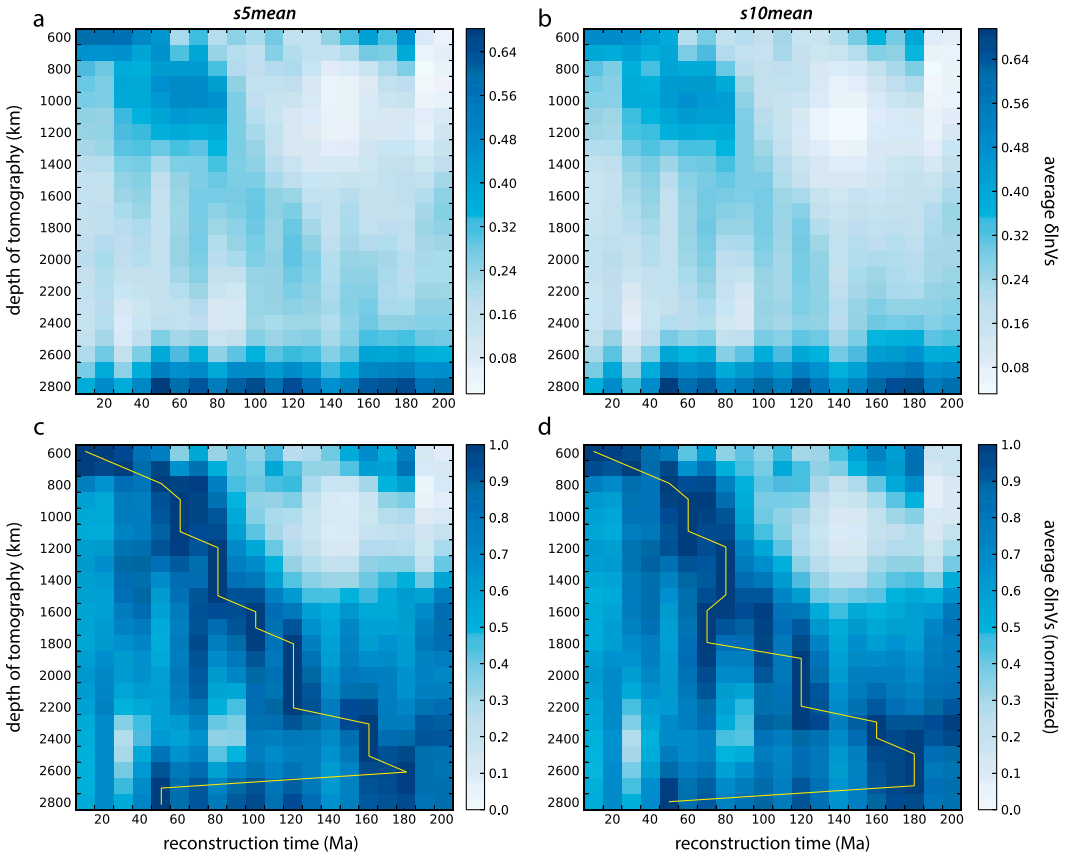

Figure 2. Average $\delta \ln V_S$-per-subduction-cell results for various time-depth comparisons between the plate model [*Seton et al.*, 2012] and the (a) s5mean and (b) s10mean tomography models [*Doubrovine et al.*, 2016], according to the process illustrated in Figure 1. (c, d) Depth normalization of Figures 2a and 2b where all average $\delta \ln V_S$ values at a given depth were divided by the maximum value from that depth. The yellow line shows the "best fit," connecting the maximum average $\delta \ln V_S$ values at each depth.

correlations and that range would be further widened by the imperfect (blurred) imaging of the slab by seismic tomography [*Ritsema et al.*, 2007] and by the effects of slab deformation [*Sigloch and Mihalynuk*, 2013] or lateral mantle flow. In the lowermost mantle (below ~1800 km), the consistently positive average $\delta \ln V_S$ values are also a consequence of the very wide spatial distribution of positive "anomalies" in all *S* wave models (Figure S2). Together these observations imply that visual cross correlation of paleo-subduction and mantle structure—including matching of tomographic observations with predictions from 3-D thermomechanical subduction models—must be done with great care as such comparisons are prone to problems with nonuniqueness and thus high uncertainty.

4. Statistical Comparisons

Remarkably, the best fit *t-d* curves of Figure 2 (which connect the reconstruction times that maximize the average $\delta \ln V_S$ value for each depth) are mostly linear between 600 and 2600 km depth, suggesting a positive correlation between reconstruction age and slab depth, with the average slope corresponding to a slab sinking rate of ~1.2 cm yr^{-1}. But how significant is this correlation, or is it just coincidence? To address this question, we perform a simple Monte Carlo test. For each *t-d* comparison we first simulate the distribution of average $\delta \ln V_S$ values under the assumption that there exists no relation between $\delta \ln V_S$ and reconstructed subduction geometries. To accomplish this, for each *t-d* comparison we rotate the reconstructed subduction geometry using a uniformly random rotation matrix [*Brannon*, 2002] and compute a new (simulated) average $\delta \ln V_S$ per subduction cell. The uniformly random rotation matrix, given a reference direction, generates sample directions that are uniformly distributed on the unit sphere. Notably, while the rotation axes of the equivalent axis-angle form of the matrix are uniformly distributed (on the unit sphere), the rotation angles

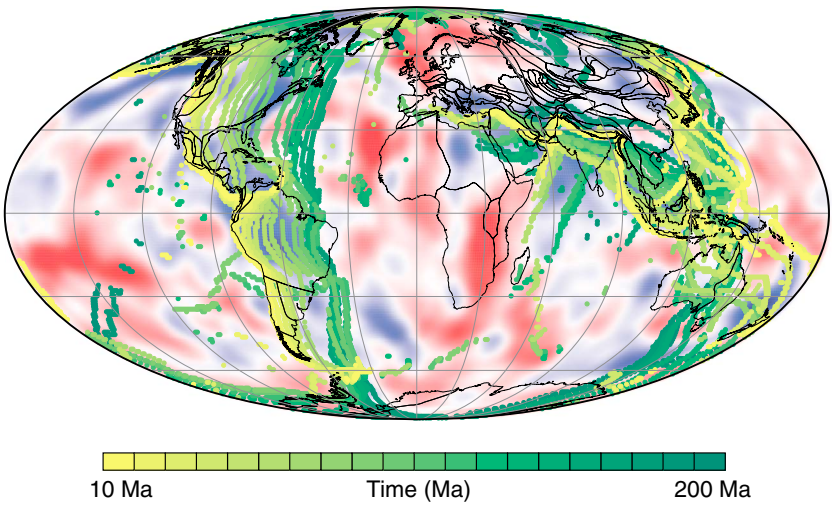

Figure 3. Subduction cells through time (10–200 Ma), as derived from the plate model of *Seton et al*. [2012] according to the process described in the text, illustrated together with an example of *S* wave tomography (at 1200 km; s10mean model [*Doubrovine et al*., 2016]). Note that with respect to the size of the positive $\delta \ln V_S$ anomalies beneath them, many subduction zones have not migrated substantially over 200 Myr. The isolated subduction cells in the east Pacific, Atlantic, and Indian Oceans are due to imperfections in the plate model; the filtering of these artifacts is discussed in the text.

are *not* uniformly distributed, but follow probability density function: $P_\alpha(\alpha) = \frac{1}{\pi}\sin^2\frac{\alpha}{\pi}, -\pi \leq \alpha \leq \pi$ [*Brannon*, 2002]. By repeating this procedure (here repeated 10^5 times), we simulate the distribution of average $\delta \ln V_S$ values under the null hypothesis that the positive values of $\delta \ln V_S$ are not related to the reconstructed locations of subduction and estimate the probability of observing an average $\delta \ln V_S$ as large or larger than the actually observed value if the null hypothesis is correct. Thus, for those *t-d* comparisons that yield an observed average $\delta \ln V_S$ value in excess of 99% of the simulated values, the null hypothesis can be rejected at the 1% significance level (i.e., the estimated probability is less than 1%). In Figure 4 we plot the results of those *t-d* comparisons for which the null hypothesis can be rejected at the 1% significance level. Examples of the simulated distributions from several profiles across the *t-d* comparison space are presented in the supporting information (Figure S3).

Above 2000 km depth, the null hypothesis cannot be rejected (at the 1% significance level) for *t-d* comparisons corresponding to slab sinking rates slower than ~1.1 cm yr^{-1}. Although extremely high sinking rates would seem to be permissible from the broad range of significant results at 30 and 40 Ma, we note that such solutions are not as continuous as they are for slower sinking rates, and we interpret them as artifacts due to imperfections in both the plate and tomographic models. Indeed, the fastest slab sinking rate that can be projected continuously and linearly through the region corresponding to the 1% significance level in the lower mantle is ~1.9 cm yr^{-1}. Faster rates could be projected through the upper lower mantle (above ~1800 km) but would require a break in slope to proceed at slower rates below 1800 km. In the deeper mantle, at 2500 and 2600 km depth, the s10mean tomography model [*Doubrovine et al*., 2016] yields significant comparisons at 180 Ma, but these are not reflected in the majority of the individual tomography models when considered independently. Notably, inclusion of these comparisons in the slab sinking rate calculation would further constrain the rate to ~1.1–1.4 cm yr^{-1} (if constant through the entire lower mantle), or require a change in sinking rate in the lowermost mantle. Although we do not explicitly consider the upper mantle herein, the significant comparisons at 600 km suggest that subducted slabs generally sink to the base of the upper mantle in 10 to 40 Myr, reflecting a reasonable average upper mantle sinking rate of 1.5 to 6 cm yr^{-1}.

5. Sensitivity Tests

In addition to the experiments described above, we conducted a variety of sensitivity tests to consider the effects and possible biases associated with our data selection and definitions. We have preferentially used the s5mean and s10mean tomography models in an attempt to amplify the signal-to-noise ratio in the

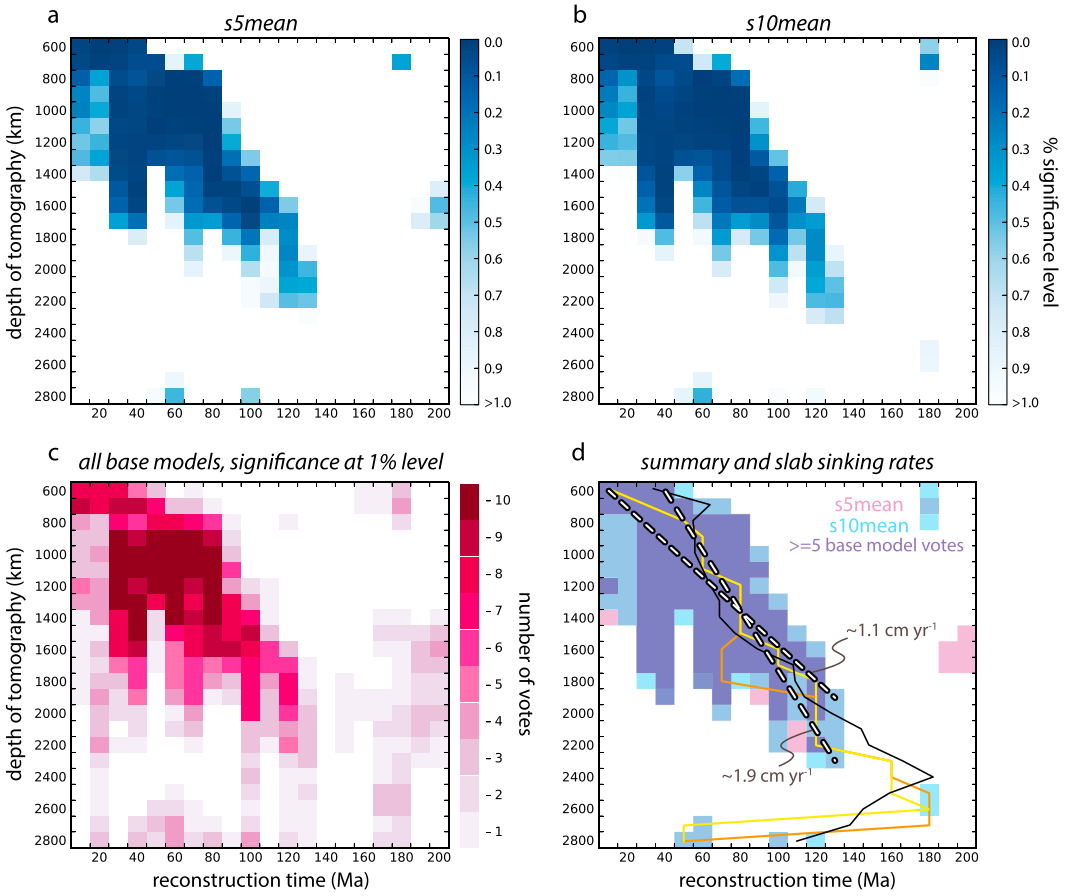

Figure 4. Time-depth comparisons (using the (a) s5mean and (b) s10mean tomography models [*Doubrovine et al.*, 2016]) for which the null hypothesis of randomness can be rejected at the 1% significance level. (c) Same as in Figures 4a and 4b but with all 10 of the individual global *S* wave tomography models considered individually, with the results displayed as a voting map. A vote of "10" means that for a given time-depth comparison the correlation was significant at the 1% level in all 10 models. (d) A composite of the results from s5mean, s10mean, and the individual tomographic models, together with the s5mean and s10mean best fit curves (yellow and orange lines, respectively) and the average best fit computed from the 10 individual base models (black line). The thick dashed lines show the bounding linear solutions for the average slab sinking rate described in the text.

mantle structure inferred from the individual *S* wave tomography models. To further consider the possible biasing effects of noise in the tomography models, we have explored the results of filtering them by two different approaches. In both cases the filtering was applied after extraction of depth slices from the tomographic models and the resampling of the $\delta \ln V_S$ values to the geographic grid. In the first approach we employed a constant truncation level, wherein all $\delta \ln V_S$ values below 0.4% were zeroed. In the second approach the standard deviation of $\delta \ln V_S$ was determined for each layer *d*, and all $\delta \ln V_S$ values within 1 standard deviation of 0 were then zeroed. A summary of the results of these experiments are shown in Figure S4. Although the *t-d* comparisons for some (individual) *S* wave tomography models changed significantly with filtering, the significant *t-d* trend among the collection of models remained largely the same, albeit degraded. The most notable difference after filtering is that no *t-d* comparisons below a depth of 1900 km are significant at the 1% level for the majority of the individual models.

To consider the sensitivity of our results to the selected plate model, we refitted the model of *Seton et al.* [2012] to the absolute plate motion framework of *Doubrovine et al.* [2012], extended to 200 Ma with the paleomagnetic true polar wander corrected reference frame of *Torsvik et al.* [2014], and repeated the *t-d* comparison experiments (Figure S5). The resulting best fit curves from the simple *t-d* comparisons of the refitted plate model to the s5mean and s10mean tomography models show agreement with the original results of Figure 2. To consider the effect of our preferred practical definition of subduction, we repeated our initial

comparison experiment with a range of alternative settings for the relative motion (transcurrent versus convergent) and absolute convergence value thresholds (Figure S6). The resulting best fit curves are again largely in agreement with those of Figure 2, indicating that the results of our analyses are not strongly sensitive to our preferred definition of subduction (i.e., our filtering of the convergent cells in the plate model).

Finally, we repeated the simple and statistical comparison experiments with the use of the weighted median rather than the weighted average, and the results were highly similar to those of the original experiments, verifying that our findings are not contingent on the selection of test statistic.

6. Implications

The results of our Monte Carlo test demonstrate that a statistically significant correlation exists between reconstructed locations of subduction (back to 130 Ma) and mantle structure as derived from seismic tomography (between 600 and 2300 km depth), which we interpret as an equivalent correlation between positive lower mantle seismic anomalies and remnants of subduction. The correlation is time-depth progressive and approximately linear, suggesting that the concept of a globally averaged lower mantle slab sinking rate is viable, to the first order. Because our analysis yields an envelope of statistically significant time-depth comparisons, we are unable to exactly establish the "true" global average slab sinking rate, but from the range of rates that are permissible, we can conclude that the global average lies between ~1.1 and 1.9 cm yr^{-1}, assuming slabs sink at a mostly constant rate through the lower mantle. If the rate of sinking is not constant, faster rates are possible above 1800 km, but sinking would have to slow (or slabs would have to temporarily stagnate) at or above 1800 km depth. Likewise, slower rates are possible (or slabs could consistently stagnate) above 1000 km, but sinking would have to proceed more rapidly below. More complex nonlinear sinking profiles are also possible, including those in which slabs would slow or temporarily stagnate at depths where phase transitions or compositional boundaries have been suggested (e.g., ~660 and 1000 km depth [*Ballmer et al*., 2015]) but are not required within the present uncertainties. As the correlation between 600 and 2300 km depth exhibits a linear trend, we prefer the simplest interpretation of a relatively constant sinking rate, although we note that a nonlinear sinking rate is more likely in reality. Our range of linear sinking rates overlaps both the previous empirical estimates of 1.2 ± 0.3 cm yr^{-1} [*van der Meer et al*., 2010] or 1.3 ± 0.3 cm yr^{-1} [*Butterworth et al*., 2014], and the 2.0 ± 0.8 cm yr^{-1} average sinking rate suggested by geodynamic models run with a mantle viscosity structure derived from mineral physics and surface observations [*Steinberger and Calderwood*, 2006; *Steinberger et al*., 2012]. That our range of rates overlaps these two is intriguing because an average slab sinking rate of 1.2 cm yr^{-1} is difficult to accommodate through self-consistent modifications to the mantle viscosity structure of *Steinberger and Calderwood* [2006], yet comparisons between seismic tomography and the results of geodynamic models using that viscosity model suggest that an average slab sinking rate of 2.0 cm yr^{-1} may be too fast [*Steinberger et al*., 2012]. Our range of average slab sinking rates thus bridges empirical [*van der Meer et al*., 2010; *Butterworth et al*., 2014] and model-derived sinking rates [*Steinberger et al*., 2012] and, following *Čížková et al*. [2012], may be used to further explore the uncertainty limits on our estimates of lower mantle viscosity.

The finding of a significant correlation between mantle structure and past subduction corroborates the premises of the subduction reference frame and provides it a quantitative foundation that can be refined through longitudinal "fine tuning" and evaluation against better resolved plate tectonic and tomographic models. Because longitude is poorly known prior to 83.5 Ma and is moreover undefined by hotspots prior to 130 Ma, the practical approach of estimating paleolongitude in pre-Late Cretaceous time has been to adopt the so-called "zero-longitude" Africa assumption, which presumes that Africa, having been surrounded by mid-ocean ridges since Pangea breakup, likely moved the least in longitude since, and therefore best qualifies as a longitudinally "fixed" reference plate back to the early Mesozoic [*Torsvik et al*., 2008]. Nevertheless, it is likely that Africa's longitudinal motion in the Jurassic and Early Cretaceous, if small, was not zero. Consequently, as Africa acts as the reference (or "anchor") plate under this assumption, the offset in Africa's paleolongitude is equivalent to a global offset in paleolongitude (disregarding relative longitude uncertainties). It is therefore permissible to apply time-dependent global longitudinal shifts (rotations about the spin axis) to the plate tectonic model during these times, and by applying shifts which maximize the fit between past subduction and mantle structure, global paleolongitude can be constrained in the absence of hotspot tracks [*van der Meer et al*., 2010]. However, the ubiquitous positive correlations from our initial

experiment demonstrate that such longitudinal fine tuning is prone to problems with nonuniqueness, and tradeoffs in rotation space versus reconstruction time may offer similar marginal improvements whose relative significance is difficult to assess. But a more challenging problem lies in the fact that a longitudinal shift applied to a true polar wander corrected reference frame (which is a necessary starting point) will inherently necessitate recalculation of the true polar wander of that reference frame, followed by reassessment of its fit to mantle structure, and so on. While such a labor-intensive endeavor is worthwhile and indeed paramount with regard to the determination of pre-Late Cretaceous longitudes, it is beyond the scope of the present study. Notwithstanding, our recognition of a significant correlation back to 130 Ma suggests that the zero-longitude Africa assumption is satisfactorily valid from at least that time.

Correlations between reconstructed subduction older than 130 Ma and mantle depths deeper than 2300 km are dubious in our present analysis but may be bolstered through future refinements to both the plate and tomographic models. For the plate model, this may include both revisions to the time-dependent continental reconstructions and plate boundary networks, but also alternatives to the zero-longitude Africa assumption. From the tomographic side, further correlation may be made possible through improvements to the resolution of the *S* wave models in the lowermost mantle.

Acknowledgments
This work was supported by the European Research Council under the European Union's Seventh Framework Programme (FP7/2007-2013)/ERC advanced grant agreement 267631 (Beyond Plate Tectonics) and the Research Council of Norway through its Centres of Excellence funding scheme, project 223272 (CEED). We thank Editor Jeroen Ritsema and three anonymous reviewers for improvements to the manuscript.

References

Auer, L., L. Boschi, T. Becker, T. Nissen-Meyer, and D. Giardini (2014), Savani: A variable resolution whole-mantle model of anisotropic shear velocity variations based on multiple data sets, *J. Geophys. Res. Solid Earth*, *119*, 3006–3034.

Ballmer, M. D., N. C. Schmerr, T. Nakagawa, and J. Ritsema (2015), Compositional mantle layering revealed by slab stagnation at ~1000-km depth, *Sci. Adv.*, *1*(11), e1500815.

Becker, T. W., and L. Boschi (2002), A comparison of tomographic and geodynamic mantle models, *Geochem. Geophys. Geosyst.*, *3*(1), 1003, doi:10.1029/2001GC000168.

Brannon, R. (2002), *A Review of Useful Theorems Involving Proper Orthogonal Matrices Referenced to Three-Dimensional Physical Space*, Sandia National Laboratories, Albuquerque.

Butterworth, N., A. Talsma, R. Müller, M. Seton, H.-P. Bunge, B. Schuberth, G. Shephard, and C. Heine (2014), Geological, tomographic, kinematic and geodynamic constraints on the dynamics of sinking slabs, *J. Geodyn.*, *73*, 1–13.

Čížková, H., A. P. van den Berg, W. Spakman, and C. Matyska (2012), The viscosity of Earth's lower mantle inferred from sinking speed of subducted lithosphere, *Phys. Earth Planet. Inter.*, *200*, 56–62.

Doubrovine, P. V., B. Steinberger, and T. H. Torsvik (2012), Absolute plate motions in a reference frame defined by moving hot spots in the Pacific, Atlantic, and Indian oceans, *J. Geophys. Res.*, *117*, B09101, doi:10.1029/2011JB009072.

Doubrovine, P. V., B. Steinberger, and T. H. Torsvik (2016), A failure to reject: Testing the correlation between large igneous provinces and deep mantle structures with EDF statistics, *Geochem. Geophys. Geosyst.*, *17*, 1130–1163, doi:10.1002/2015GC006044.

Goldreich, P., and A. Toomre (1969), Some remarks on polar wandering, *J. Geophys. Res.*, *74*(10), 2555–2567, doi:10.1029/JB074i010p02555.

Grand, S. P. (2002), Mantle shear–wave tomography and the fate of subducted slabs, *Philos. Trans. R. Soc. Lond. A*, *360*(1800), 2475–2491.

Gurnis, M., M. Turner, S. Zahirovic, L. DiCaprio, S. Spasojevic, R. D. Müller, J. Boyden, M. Seton, V. C. Manea, and D. J. Bower (2012), Plate tectonic reconstructions with continuously closing plates, *Comput. Geosci.*, *38*(1), 35–42.

Houser, C., G. Masters, P. Shearer, and G. Laske (2008), Shear and compressional velocity models of the mantle from cluster analysis of long-period waveforms, *Geophys. J. Int.*, *174*(1), 195–212.

Kustowski, B., G. Ekström, and A. Dziewoński (2008), Anisotropic shear-wave velocity structure of the Earth's mantle: A global model, *J. Geophys. Res.*, *113*, B06306, doi:10.1029/2007JB005169..

Masters, G., G. Laske, H. Bolton, and A. Dziewonski (2000), The relative behavior of shear velocity, bulk sound speed, and compressional velocity in the mantle: Implications for chemical and thermal structure, in *Earth's Deep Interior: Mineral Physics and Tomography From the Atomic to the Global Scale*, pp. 63–87, AGU, Washington, D. C.

Mégnin, C., and B. Romanowicz (2000), The three-dimensional shear velocity structure of the mantle from the inversion of body, surface and higher-mode waveforms, *Geophys. J. Int.*, *143*(3), 709–728.

Montelli, R., G. Nolet, F. Dahlen, and G. Masters (2006), A catalogue of deep mantle plumes: New results from finite-frequency tomography, *Geochem. Geophys. Geosyst.*, *7*, Q11007, doi:10.1029/2006GC001248.

Richards, M. A., and D. C. Engebretson (1992), Large-scale mantle convection and the history of subduction, *Nature*, *355*(6359), 437–440.

Ritsema, J., A. K. McNamara, and A. L. Bull (2007), Tomographic filtering of geodynamic models: Implications for model interpretation and large-scale mantle structure, *J. Geophys. Res.*, *112*, B01303, doi:10.1029/2006JB004566.

Ritsema, J., A. Deuss, H. J. Van Heijst, and J. H. Woodhouse (2011), S40RTS: A degree-40 shear-velocity model for the mantle from new Rayleigh wave dispersion, teleseismic traveltime and normal-mode splitting function measurements, *Geophys. J. Int.*, *184*(3), 1223–1236.

Scrivner, C., and D. L. Anderson (1992), The effect of post Pangea subduction on global mantle tomography and convection, *Geophys. Res. Lett.*, *19*(10), 1053–1056, doi:10.1029/92GL00864.

Seton, M., R. D. Müller, S. Zahirovic, C. Gaina, T. H. Torsvik, G. Shephard, A. Talsma, M. Gurnis, M. Turner, and S. Maus (2012), Global continental and ocean basin reconstructions since 200 Ma, *Earth Sci. Rev.*, *113*(3), 212–270.

Sigloch, K., and M. G. Mihalynuk (2013), Intra-oceanic subduction shaped the assembly of Cordilleran North America, *Nature*, *496*(7443), 50–56.

Simmons, N. A., A. M. Forte, and S. P. Grand (2007), Thermochemical structure and dynamics of the African superplume, *Geophys. Res. Lett.*, *34*, L02301, doi:10.1029/2006GL028009.

Simmons, N. A., A. M. Forte, L. Boschi, and S. P. Grand (2010), GyPSuM: A joint tomographic model of mantle density and seismic wave speeds, *J. Geophys. Res.*, *115*, B12310, doi:10.1029/2010JB007631.

Steinberger, B., and A. R. Calderwood (2006), Models of large-scale viscous flow in the Earth's mantle with constraints from mineral physics and surface observations, *Geophys. J. Int.*, *167*(3), 1461–1481.

Steinberger, B., T. H. Torsvik, and T. Becker (2012), Subduction to the lower mantle—A comparison between geodynamic and tomographic models, *Solid Earth*, *3*(2), 415–432.

Torsvik, T. H., R. D. Müller, R. Van der Voo, B. Steinberger, and C. Gaina (2008), Global plate motion frames: Toward a unified model, *Rev. Geophys.*, *46*, RG3004, doi:10.1029/2007RG000227.

Torsvik, T. H., R. Van der Voo, U. Preeden, C. Mac Niocaill, B. Steinberger, P. V. Doubrovine, D. J. J. van Hinsbergen, M. Domeier, C. Gaina, and E. Tohver (2012), Phanerozoic polar wander, palaeogeography and dynamics, *Earth Sci. Rev.*, *114*(3), 325–368.

Torsvik, T. H., R. van der Voo, P. V. Doubrovine, K. Burke, B. Steinberger, L. D. Ashwal, R. G. Trønnes, S. J. Webb, and A. L. Bull (2014), Deep mantle structure as a reference frame for movements in and on the Earth, *Proc. Natl. Acad. Sci. U.S.A.*, *111*, 8735–8740.

van der Meer, D. G., W. Spakman, D. J. J. van Hinsbergen, M. L. Amaru, and T. H. Torsvik (2010), Towards absolute plate motions constrained by lower-mantle slab remnants, *Nat. Geosci.*, *3*(1), 36–40.

Wen, L., and D. L. Anderson (1997), Slabs, hotspots, cratons and mantle convection revealed from residual seismic tomography in the upper mantle, *Phys. Earth Planet. Inter.*, *99*(1), 131–143.

Zahirovic, S., M. Seton, and R. Müller (2014), The Cretaceous and Cenozoic tectonic evolution of Southeast Asia, *Solid Earth*, *5*(1), 227–273.